Nanoscale Horizons

ROYAL SOCIETY OF CHEMISTRY

COMMUNICATION

View Article Online
View Journal | View Issue

Cite this: *Nanoscale Horiz.*, 2025, 10, 1414

Received 11th March 2025,
Accepted 22nd April 2025

DOI: 10.1039/d5nh00142k

rsc.li/nanoscale-horizons

Advancing green electronics: tunable piezoelectric enhancement in biodegradable poly(L-lactic acid) PLLA films through thermal-strain engineering†

Youssif Merhi, *[a] Vincent Goumarre,[a] Konstantin Romanyuk,[b] Yasith Amarasinghe,[a] Andrei Kholkin, [bc] Pernille Klarskov[a] and Shweta Agarwala *[a]

The rising interest in biodegradable polymers like PLLA is gaining attention for their potential in next-generation biomedical devices. One of the critical challenges in leveraging PLLA's full potential is enhancing its crystallinity, as it greatly influences mechanical, thermal, degradation, and piezoelectric properties, which are essential for various applications. Here, we use thermal annealing and strain engineering to transform the amorphous phase into a more ordered crystalline structure. Through various characterization techniques, we show that crystallinity increased progressively from 34.8% in unprocessed films to 57.4% at 100% strain. Terahertz time-domain spectroscopy is employed to gain insights into the structural and dynamic properties where we study low-frequency molecular vibrations and anisotropic properties, enabling simultaneous evaluation of structural, such as crystallinity, and optical characteristics. Rotational analysis provides direct evidence of molecular orientation and birefringence induced by mechanical processing. These findings align strongly with the traditional characterization techniques (XRD, WAXS, DSC, and FTIR). Piezoresponse force microscopy shows that the VPFM signal increased from 0.65 ± 0.15 pm V^{-1} in unprocessed films to 6.5 ± 1.5 pm V^{-1} at 100% strain. The in-depth work is an important step in gaining a deeper understanding of how the crystalline regions form, evolve under different processing conditions, and influence PLLA's overall properties.

New concepts

This study proposes new insights into how molecular alignment affects electrical and structural properties by understanding the interplay between molecular orientation, birefringence and crystallinity in biodegradable polymers, crucial for next-generation piezoelectric applications. It presents a novel approach of strain engineering *via* mechanical stretching at room temperature (unlike the published literature) to progressively increase the crystallinity of PLLA; thus making the process more sustainable and energy-efficient. The study also builds a new hybrid analytical framework for biodegradable polymers by integrating emerging terahertz spectroscopy (THz-TDS) with conventional techniques (XRD, WAXS, DSC, and FTIR) to provide a comprehensive understanding of polymer microstructure and functional properties.

Introduction

Poly(L-lactic acid) (PLLA) is a biodegradable, biocompatible polymer that has garnered significant attention in biomedical applications such as tissue engineering and implantable sensors due to its tunable mechanical and piezoelectric properties.[1–3] However, the intrinsic piezoelectric performance of PLLA remains suboptimal for emerging biomedical sensing technologies, primarily due to limitations in molecular alignment and crystallinity.[3–5] Enhancing its piezoelectric response is critical for converting biomechanical signals into electrical outputs. However, this requires a deeper understanding of structure–property relationships and efficient, scalable processing strategies.[6–8] Current methods to improve PLLA's piezoelectricity rely heavily on high-temperature treatments and complex chemical modifications, often compromising its biodegradability or limiting practical implementation.[1,9–12] Moreover, the electromechanical response of PLLA is strongly influenced by its crystalline phase transitions, particularly the transformation from the α-phase (with disordered dipole orientation) to the β-phase (with aligned dipoles) *via* mechanical strain.[13–17] Yet, accurate quantification of these phase changes and their influence on piezoelectricity remains elusive.

This complexity arises from the inherent piezoelectric properties of PLLA, which are due to its low symmetry, highly ordered structures, and the absence of an inversion center It can be obtained easily *via* melting or solution-phase crystallization methods.[13,14,18] The β-phase, which has a left-handed

[a] *Department of Electrical and Computer Engineering, Aarhus University, Finlandsgade 22, 8200, Aarhus, Denmark. E-mail: Youssifm@ece.au.dk, shweta@ece.au.dk*

[b] *CICECO-Institute of Materials and Department of Physics, Campus de Santiago, University of Aveiro, Aveiro, 3810-193, Portugal*

[c] *Institute of Solid State Physics, University of Latvia, LV-1063 Riga, Latvia*

† Electronic supplementary information (ESI) available. See DOI: https://doi.org/10.1039/d5nh00142k

3_1 helical conformation and an orthorhombic or triclinic unit cell, can be produced by controlling the post-process drawing and annealing conditions.[1] The C═O dipoles of α-PLLA are generally oriented in all directions (360°) along the main chain of the helical structure, resulting in a zero net-dipole moment. α-PLLA can be transformed into β-PLLA by stretching or drawing processes.[13,19] The C═O dipoles of β-PLLA are aligned along the backbone chain, so the total dipole moment is significantly increased. The thermal, mechanical, and electrical properties of PLLA are significantly dependent on the crystalline phases it contains.[16]

Given the importance of crystalline phases in determining PLLA's properties, it is crucial to use advanced techniques to study the phases and their transitions. Recently, terahertz (THz) spectroscopy has gained popularity due to its ability to probe intermolecular and low-energy intramolecular molecular vibrations.[20–23] THz spectroscopy can detect weak intermolecular forces such as hydrogen bonds and van der Waals interactions, making it ideal for studying the subtle changes in the crystalline structure caused by mechanical strain.[22,24,25] In THz time-domain spectroscopy (THz-TDS), coherent THz pulses with a linear polarization are used to measure the dielectric properties of materials. Rotating the material relative to the THz polarization direction allows for sensing of anisotropic effects offering a detailed analysis of how molecular alignment affects PLLA's piezoelectric response.[26–31] Additionally, THz radiation is non-invasive and poses no significant harm, particularly when compared to X-rays, which are commonly used for crystallinity studies.[32,33]

Although several qualitative and quantitative THz spectroscopic studies of polylactic acid (PLA) have been conducted to study the crystallization process and the birefringence of strain-induced crystallization,[28–30,34] quantitative estimation of crystallinity and detailed analyses of PLLA, particularly regarding the improvement of crystallinity for piezoelectric enhancement, are still lacking. This study addresses these gaps through a novel, energy-efficient approach that induces crystallinity and molecular alignment in PLLA films *via* ambient-condition mechanical stretching. Unlike conventional methods that require high temperatures to soften the material for stretching and inducing molecular alignment, our approach achieves controlled stretching under ambient conditions thus utilizing energy-efficient processing that can be up-scaled. Crucially, we integrate terahertz time-domain spectroscopy (THz-TDS), a non-destructive, highly sensitive tool capable of probing low-energy molecular vibrations, with complementary techniques such as XRD, WAXS, DSC, and FTIR to map the structural evolution of PLLA at multiple scales. THz-TDS offers a unique advantage by enabling full angular analysis of anisotropy and molecular orientation, providing insights inaccessible through traditional methods. Our work delivers a comprehensive and quantitative assessment of post-processed PLLA films, establishing clear correlations between strain-induced crystalline phases and enhanced piezoelectric performance. This integrated spectroscopic strategy not only advances the fundamental understanding of PLLA's structure–property dynamics but also paves the way for sustainable, high-performance, biodegradable piezoelectric sensors, contributing to next-generation green medical electronics. Ultimately, this research seeks to optimize PLLA films for enhanced piezoelectric performance, facilitating the development of advanced biomedical sensors, and potentially broadening the application scope of PLLA-based piezoelectric devices.

Methods

Materials

PLLA granules (PURASORB PL 24) were obtained from Corbion. Before use, the granules were subjected to overnight drying at 80 °C in a vacuum oven. Chloroform (Merck) was utilized as the solvent for PLLA dissolution.

Preparation of PLLA films

To create PLLA films, 10 grams of PLLA granules were dissolved in 50 grams of chloroform. Chloroform plays a crucial role in the synthesis process by enabling the fabrication of high-quality PLLA films under ambient conditions. Its moderate evaporation rate and strong solubility for PLLA help ensure uniform film formation with minimal defects. The resulting mixture was stirred for 4 hours at room temperature at 200 RPM until complete dissolution. The solution was stored overnight in a refrigerator at 4 °C to prevent bubble formation. The cold PLLA solution was poured into a glass Petri dish and air-dried for 4 hours at room temperature. The resulting PLLA film was carefully peeled from the Petri dish and cut into rectangular pieces measuring 15 × 50 or 50 × 50 mm. Subsequently, the pre-cut films underwent a uniaxial drawing process, achieving strain % from 50–100%. The strain was calculated using the formula:

$$\text{Strain } (\%) = \frac{L - L_0}{L_0} \times 100$$

where L_0 is the initial length of the sample and L is the final length after stretching. This method offers a clear and direct measure of deformation. The uniaxial stretching of the films was carried out at room temperature using a Zwick/Roell Z050 tensile testing machine. The process began with an initial speed of 50 mm min^{-1} and a pre-load of 0.1 MPa applied at a speed of 5 mm min^{-1}. The tensile modulus was set at 1 mm min^{-1}, followed by a stretching speed of 20 mm min^{-1}. After stretching, the films were fixed at their strained length and heat-treated for 8 hours at 80 °C. Following heat treatment, the films were rapidly quenched in an ice bath for 7 hours to ensure structural stability.

Characterization

Scanning electron microscopy (SEM). Images were acquired using the FEI Magellan 400 SEM. A 10 nm Ti coating was applied using the Cryofox Explorer 500 GLAD from Denmark to improve image quality and prevent charging.

Differential scanning calorimetry (DSC). DSC was conducted using the Thermal Analysis Mettler Toledo DSC3 (USA) with an autosampler to explore the thermal behavior and crystallinity degree of our material. The heat flow was measured in the range of 25 to 200 °C at a rate of 10 °C min^{-1} under a nitrogen gas atmosphere.

Fourier-transform infrared (FTIR) spectroscopy. FTIR spectra were recorded using a Bruker Alpha II Platinum ATR spectrometer. This instrument identifies molecular bonds through selective absorbance by measuring each sample's response within the range of 4000–400 cm^{-1}.

Terahertz time-domain spectroscopy (THz-TDS). THz-TDS analysis was conducted using the Toptica TeraFlash pro system, capable of measuring the THz spectrum ranging from 0.1 THz to 6 THz. Samples were introduced into the THz system after purging the setup with dry air to minimize absorption due to humidity. The THz spectrum of each sample was recorded at room temperature, with dry air without any sample serving as the reference. Each measurement comprised 1000 averages with one average taken in 180 seconds in a 200 ps time window, see Fig. S1 (ESI†). Averaging is done to increase the signal-to-noise ratio of the signal. Samples were securely affixed to the holder covering the aperture, allowing for rotational scanning (Fig. 4(a)). The stretching direction was designated as the reference point, set at 0 degrees (y direction), and considered perpendicular to the electric field polarization (x direction) of the system. For the quantification of the content of crystallinity; we used an optimized THz-TDS method, building on the foundational work of Hirata *et al.*[29] and refined using the correction algorithm by Dorney *et al.*[35] to account for internal reflections (Fabry–Perot effect). This approach enabled accurate extraction of refractive index and absorption spectra, even for thin samples where the exact sample thickness is unknown. A two-mode Lorentz oscillator model was applied, with one mode representing the crystalline phase and the other capturing the amorphous phase. This method provided precise crystallinity estimates for PLLA samples subjected to various treatments, highlighting the structural evolution of the polymer under mechanical and thermal processing.

X-ray diffraction (XRD). The PLLA film samples were assessed through one-dimensional X-ray diffraction measurements using the Bruker B8 Insitu-GIWAXS in the reflection mode, operated with the Cu cathode Kα radiation (λ = 1.5418 Å). The scan range was $10^\circ < 2\theta < 35^\circ$, and the scan speed was 10° min^{-1}.

Wide angle X-ray scattering (WAXS). Wide angle X-ray scattering (WAXS) carried out using the Xeuss 3.0 (Xenocs, France) equipped with the Genix3D micro-focus X-ray Cu Kα source. The X-ray wavelength is 1.54 Å (50 kV and 0.6 mA). The distance from the sample for WAXS are 43, 300, and 900 mm, respectively. The exposure time was 2 and 30 min for WAXS. All scattering reflections were collected under vacuum at room temperature.

Piezoresponse force microscopy (PFM). The piezoelectric response of polymer PLLA films was investigated by piezoresponse force microscopy (PFM), using a Ntegra Aura Atomic Force Microscope (NT-MDT, the Netherlands) equipped with an external HF2LI Lock-in Amplifier (Zurich Instruments, Switzerland). PFM measurements were performed with conductive Cr/Pt-coated Tap190E-G cantilevers (Budget sensors, Bulgaria) with a spring constant of 48 N m^{-1} and resonance frequency of 190 kHz. The piezoelectric response of the films was recorded in a contact mode at a frequency of 21 kHz and AC excitation voltages in the range from 4 V to 40 V. The calibration of the lateral signal was performed by means of a Y-cut quartz crystal with a shear coefficient d_{26} = 4.6 pm V^{-1}. The calibration of the vertical signal was conducted using a Z-cut single crystal of periodically poled lithium niobate (PPLN, Labfer Ltd, Russia) with longitudinal coefficient d_{33} = 6 pm V^{-1}. Each PFM image includes amplitude and phase data, revealing the piezoelectric coefficient (proportional to local polarization) and domain polarization orientation, respectively. The out-of-plane and in-plane components of the piezoresponse were measured through complementary approaches: vertical PFM (VPFM) and lateral PFM (LPFM). PLLA primarily exhibits shear piezoelectricity, known as the d14 mode, rather than the longitudinal d_{33} mode. In our study, we cut the films at a 45-degree angle relative to the molecular orientation, which we determined with high precision using THz-TDS. This allowed us to induce a shear response using a normal force, effectively enabling an apparent d_{33} measurement, although the overall response remains lower due to the material's intrinsic properties.

Results and discussion

We employed mechanical stretching and thermal annealing techniques to systematically investigate the impact of post-processing on the crystallinity and structural properties of PLLA films. Fig. 1A is a schematic representation of polymer chain orientation and the corresponding changes in crystallinity resulting from uniaxial drawing. PLLA films were subjected to uniaxial stretching at 50%, 75%, and 100% strains, as illustrated in Fig. 1B. The primary objective of the uniaxial stretching and thermal annealing was to enhance the piezoelectric properties of PLLA by increasing its crystallinity and inducing phase transitions, thereby advancing the development of more effective biomedical devices.

Scanning electron microscopy (SEM) examination revealed a significant absence of discernible morphological alterations in the unprocessed film (Fig. 1C(1)). Conversely, distinctive structures with uniform directions became visible upon applying strain, highlighting a distinct morphology in PLLA films. The number of discernible structures was directly correlated to the applied strain, implying that these structures may stem from crystalline alignment (Fig. 1C(2)–(4)).

Differential scanning calorimetry (DSC) analysis revealed significant changes in the thermal properties of PLLA films subjected to various strain levels. Initially, the unprocessed PLLA exhibited an endothermic peak at 179 °C, indicative of a melting transition (Fig. 2A). Additionally, an exothermic peak was observed at 78 °C (see Fig. 2A), which can be explained by one of two potential mechanisms: the transformation from the amorphous phase to the crystalline phase, normally described by the cold crystallization (Tcc),[36,37] or the transition from the metastable α′ phase to the thermodynamically stable α phase.[19] Based on the observed material behavior, the latter appears more likely, as the solvent evaporation during casting likely restricts molecular mobility, favoring the formation of the metastable α′ phase.[19] Upon reheating, sufficient thermal energy enables structural reorganization into the stable α phase, aligning with similar

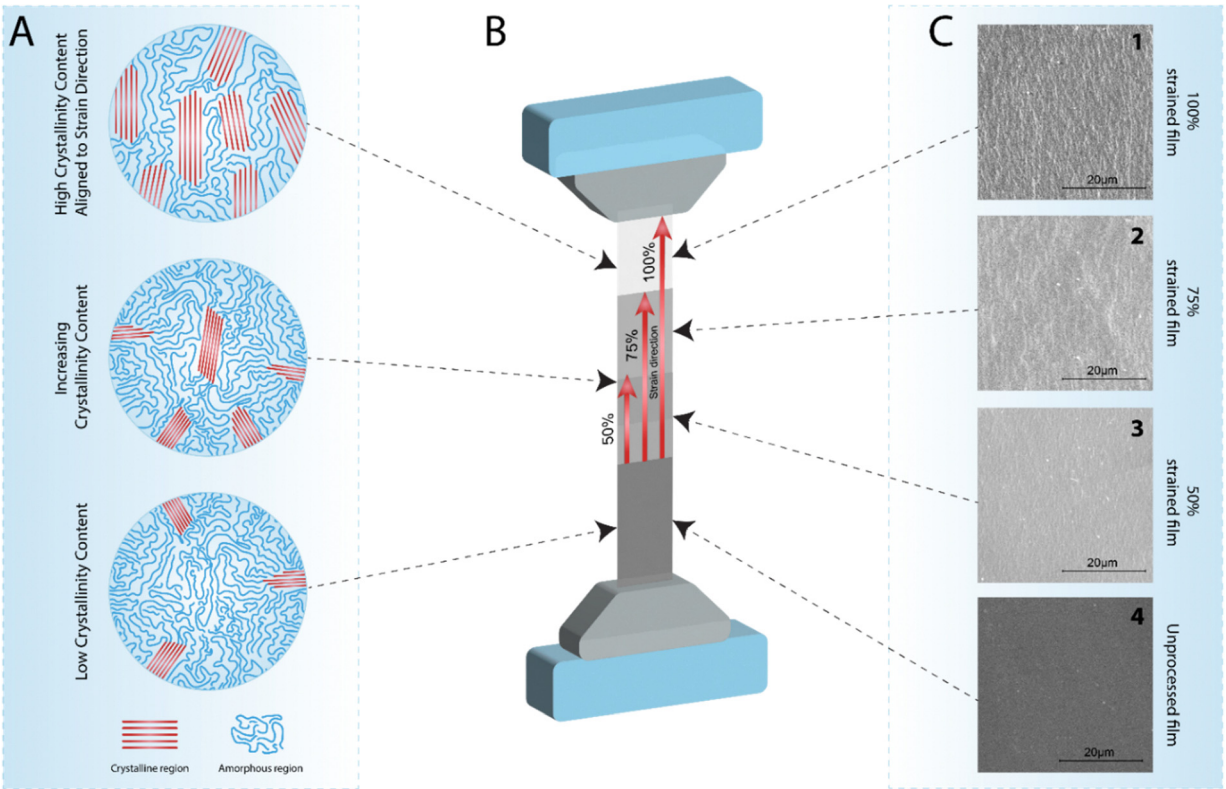

Fig. 1 (A) Illustration of the polymer orientation and the corresponding changes in crystallinity due to this post-processing of casted film. (B) Illustration of the Uniaxial stretching post-processing method. (C) SEM images of the unprocessed and strained films.

transitions reported for PLLA.[19] While Tcc typically occurs in polymers with slow crystallization kinetics, where insufficient time during cooling prevents full crystallization,[37] the casting process in this study may similarly limit molecular mobility, resulting in either residual amorphous regions or a metastable α′ phase.[19] Further characterization is required to confirm the precise mechanism. As strain increased to 50%, 75%, and 100%, the melting temperature (T_m) shifted to lower values from 179 °C to 173 °C. The gradual decrease in melting temperature with increasing strain is likely related to the formation of the β-crystalline phase, which is known to exhibit lower thermal stability compared to the α-phase, as well as to changes in molecular packing and crystallite size resulting from strain-induced alignment.[16,19,38] In our study, the observed shift in melting temperatures with increased strain appears to correlate with changes in crystalline structure. While this observation may indicate phase transitions from α to β forms, as supported by the absence of the exothermic peak in strained films, other factors such as molecular orientation, crystallite size, or strain-induced defect reduction may also contribute to these thermal changes. Further analysis integrating multiple characterization methods is necessary to confirm the specific influence of phase transitions. The inset of Fig. 2A presents the derived heat of melting values obtained from DSC data, showing a clear trend of increase from 36.12 J g^{-1} in the unprocessed film to 47.82 J g^{-1}, 52.02 J g^{-1}, and 58.45 J g^{-1} for films strained to 50%, 75%, and 100%, respectively. These results were used to calculate the crystallinity content, which will be discussed later in this paper.

FTIR spectroscopy supported the findings from DSC. The unprocessed PLLA displayed characteristic peaks at 1750 V cm^{-1} (C═O stretching) and around 1180 and 1090 cm^{-1} (C–O–C stretching).[30,39,40] The peak at 1750 cm^{-1}, corresponding to the C═O stretching vibration, exhibited a slight increase in intensity with an increasing strain% (Fig. 2B). The normalized peak intensity decreased from 0.13 for unprocessed films to 0.04 at 50% strain, 0.02 at 75% strain, and 0.01 at 100% strain. These results indicate changes in the molecular structure with strain, which may be associated with increased alignment and changes in crystallinity. Furthermore, there is a correlation between the intensity of this peak and the applied strain.[39] These FTIR changes align with the shift to higher melting temperatures and the thermal properties observed in DSC, confirming the structural reorganization of PLLA films.

Although FTIR spectroscopy provided some valid data to confirm the results obtained from DSC, no other significant insights were observed. This limitation arises because FTIR is primarily designed to analyze chemical bonds and lacks sensitivity to bulk structural changes and intermolecular interactions.[41] To address this gap, we employed THz spectroscopy, a technique uniquely suited to probing low-frequency vibrations and intermolecular forces.[22,24,25] With its ability to investigate phenomena such as hydrogen bonding networks and van der Waals interactions, THz spectroscopy is far more sensitive to changes induced by post-processing. This heightened sensitivity makes THz spectroscopy particularly effective for detecting structural transformations,

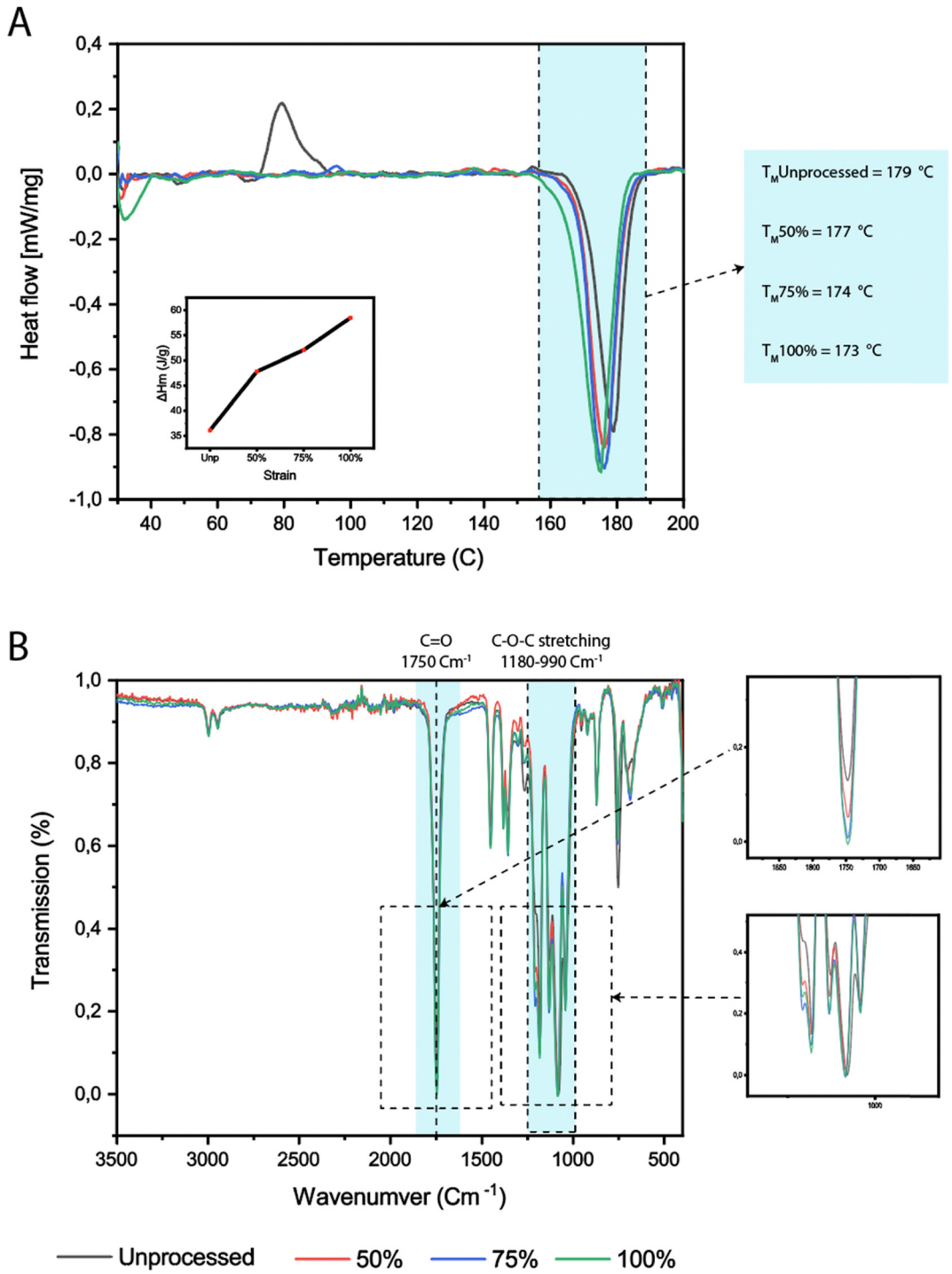

Fig. 2 (A) DSC data of the unprocessed and differently strained films. The melting temperature (T_m) is highlighted with a blue border, and the melting temperatures corresponding to each strain are indicated beneath the figure. (inset) Heat of melting (ΔH_M) plotted as a function of strain percentage, used to determine crystallinity content. (B) FTIR data of the unprocessed and differently strained films. (inset) Enlarged views of the regions are indicated by dashed boxes.

including crystallinity increases, as well as studying molecular orientation (isotropy and anisotropy) and phase changes, which are critical aspects of our analysis.

While the traditional characterization techniques have provided robust evidence of structural changes and enhanced crystallinity, THz-TDS offers additional confirmation and insights. Applying THz-TDS to the same PLLA films aims to validate the DSC and FTIR findings and further explore the material's structural properties. Also, THz-TDS provided additional insights into the structural and electromagnetic properties of PLLA films. The time-domain profile of the electric field, E, for the unprocessed film and the 100% strained film at different rotation angles

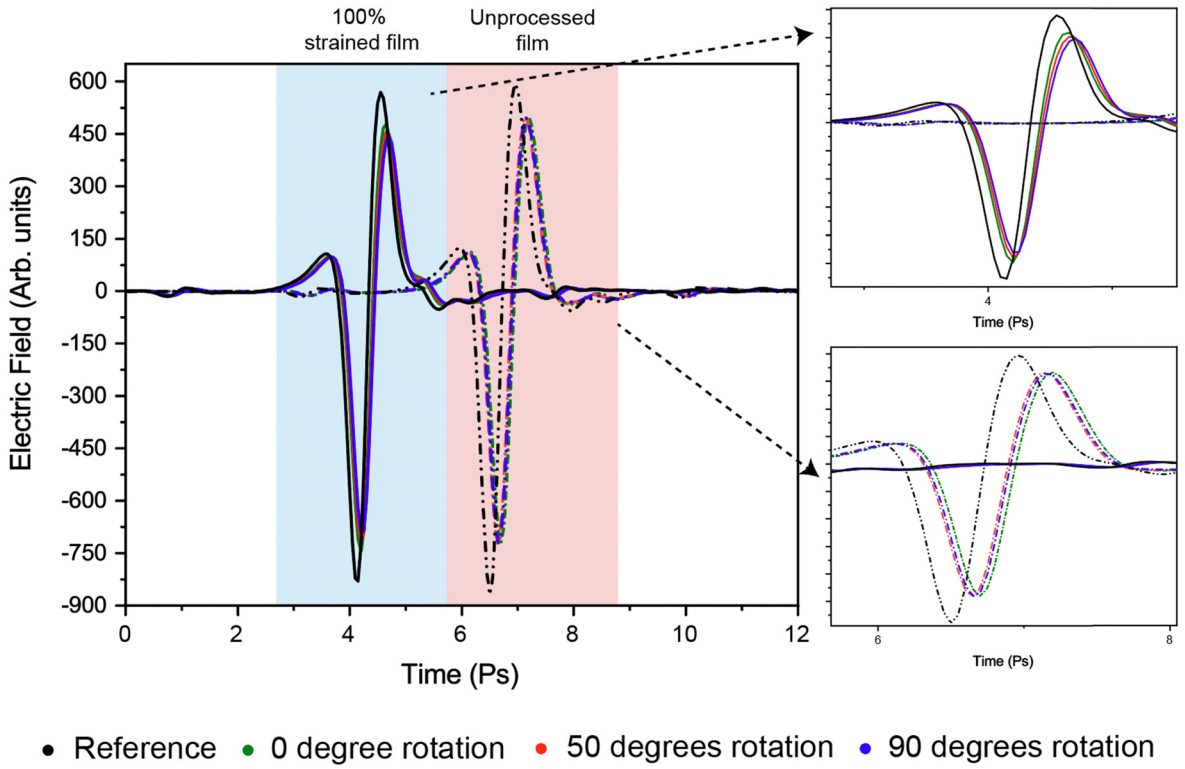

Fig. 3 THz-TDS time trace showing the electric field changes in response to strain and rotation on 100% strained PLLA film and unprocessed PLLA film. The inset provides a detailed magnification.

(0°, 50°, and 90°) is shown in Fig. 3. For the unprocessed film, no significant change in E is observed due to rotation, though the electric field is consistently reduced compared to the reference. In contrast, the 100% strained film demonstrates a clear dependence on rotation, with the most significant reduction in E observed at 90°. This result highlights the increased sensitivity of the strained film to rotation, which can be attributed to the strain-induced alignment of molecular structure within the film. Additionally, Fig. S1 (ESI†) provides an overview of the electric field profiles for all samples—unprocessed, 50%, 75%, and 100% strained films—across the full range of rotation angles from 0° to 180°. These supplementary results confirm the trends observed in Fig. 3 and further demonstrate how the degree of strain correlates with the material's sensitivity to rotation, with higher strains resulting in more pronounced changes in E.

The THz electromagnetic wave utilized in the measurements is linearly polarized, directing the electric field along a defined axis. This is utilized by the rotational sample holder used for these measurements. The film was oriented with its straining direction normal to the electromagnetic wave, allowing precise analysis at varying angles relative to the horizontally polarized electric field of the THz beam. This approach offered a detailed characterization of the material's anisotropic properties, the setup used is illustrated in Fig. 4a. The observed spectral changes provide evidence of the structural reorganization and increased crystallinity induced by mechanical stretching. Unprocessed films exhibited a consistent response in the THz electric field, marked by a uniform peak-to-peak amplitude across the rotational range (0–180 degrees), indicating isotropy (Fig. 4b). In contrast, processed films subjected to strain showed a dynamic response, with peak-to-peak amplitude evolving as a function of angular orientation. The peak intensity reached its minimum at a 90-degree rotation, aligning the strained direction with the electric field polarization (parallel) (Fig. 4b). This reduction in the peak-to-peak amplitude at 90 degrees highlights the material's pronounced anisotropy, as the molecular alignment induced by stretching enhances the interaction with the THz electric field parallel to the stretching direction, providing critical insights into its structural and dielectric properties.

The complex interplay between molecular dynamics and optical responses is explored through the analysis of absorption spectra and refractive index. Using THz-TDS measurements, the refractive index and absorption coefficient were determined employing our optimized version of the method outlined in ref. 35 and 29. We have developed a model based on Dorney's framework[35] to provide more accurate representations of refractive indices and absorption spectra without relying on a predetermined sample thickness. By employing Dorney's model as a correctional factor, our approach ensures improved precision in capturing the material's optical properties under various conditions.

This enhanced capability to characterize optical properties was instrumental in analyzing the pronounced birefringence observed in stretched PLLA films, which manifested as a difference in refractive indices along distinct axes, revealing the material's inherent anisotropy (Fig. 4c(1)–(3)). The measurements of the

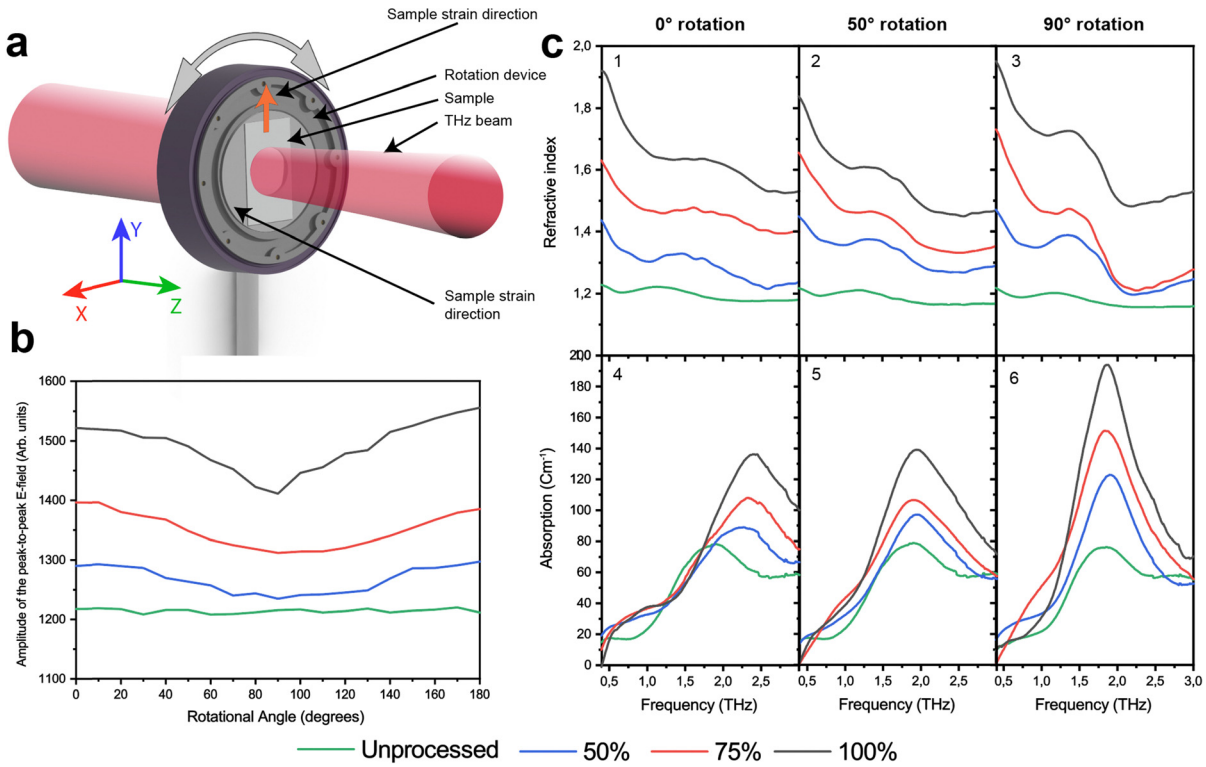

Fig. 4 (a) THz-TDS measurement setup (b) symmetric peak-to-peak amplitude over the rotational range (c) refractive index (1–3) and absorption spectra (4–6) of sample normal-, rotated 50° degrees- and parallel to the electric field polarization.

unprocessed PLLA sample exhibited no changes upon rotation, suggesting an isotropic nature with randomly oriented polymer chains and an absence of preferred molecular alignment. Moreover, the strained films exhibited significant changes in the refractive indices measured as we rotated. These experimental results indicate that at higher strains, the polymer chains in the crystalline phase are increasingly aligned along the stretching direction, enhancing the anisotropic properties of the material. Understanding the molecular orientation in processed PLLA is crucial for optimizing its piezoelectric properties, as the alignment of molecular chains directly influences the material's performance. Typically, PLLA films are cut at a 45-degree angle to the straining direction because this orientation maximizes the shear forces generated during deformation, which are necessary to produce an electrical response in materials with shear piezoelectricity like PLLA. This angle aligns the applied stress with the molecular anisotropy in such a way that it induces the strongest piezoelectric signal, as supported by theoretical models and experimental results.[1] However, due to incomplete crystallinity and non-uniform molecular alignment, the true optimal cutting angle may deviate slightly from this standard. By accurately determining the molecular orientation, we can refine the cutting process, resulting in better-aligned samples and potentially higher piezoelectric properties, leading to improved sensor performance. With THz spectroscopy, we can experimentally measure the molecular orientation, providing a precise indication of the optimal alignment for improved piezoelectric performance. In addition to this, this comprehensive analysis, by combining THz-TDS and 2D WAXS (Fig. 5B), we can provide a detailed understanding of how mechanical stretching influences the molecular orientation and crystallinity of PLLA films, ultimately affecting their optical and piezoelectric properties. With the importance of molecular orientation established, we now focus on quantifying crystallinity, a key factor influencing PLLA's piezoelectric properties. Accurate crystallinity measurements reveal structural changes from processing and their impact on performance. Here, we highlight THz spectroscopy's unique ability to complement traditional techniques like DSC for this purpose.

Simultaneously with the information gained from the refractive index, our investigation extends to the absorption spectra, revealing a distinctive peak of 1.82–1.88 THz dependent on the sample's crystallinity and orientation relative to the polarized electric field. These peaks exhibit notable sensitivity to sample rotation, as shown in Fig. 4a. More precisely, in Fig. 4c(4), at 0-degree rotation, we observe a distinctive peak in the absorption curve at 2.28 THz for the 50% strained film, 2.35 THz for the 75% strained film, and 2.41 THz for the 100% strained film, and a distinctive peak at 1.82 THz for the unprocessed film. On the other hand, in Fig. 4c(5 and 6), for rotations above 50 degrees, we observe similar peak positions at 1.88 THz for the unprocessed film and a slight shift to higher frequencies for processed films at 1.92 THz. In unprocessed samples, the absence of change in peak position and shape at all rotations signifies a uniform molecular arrangement, indicating a more isotropic configuration than stretched films, similar to previous

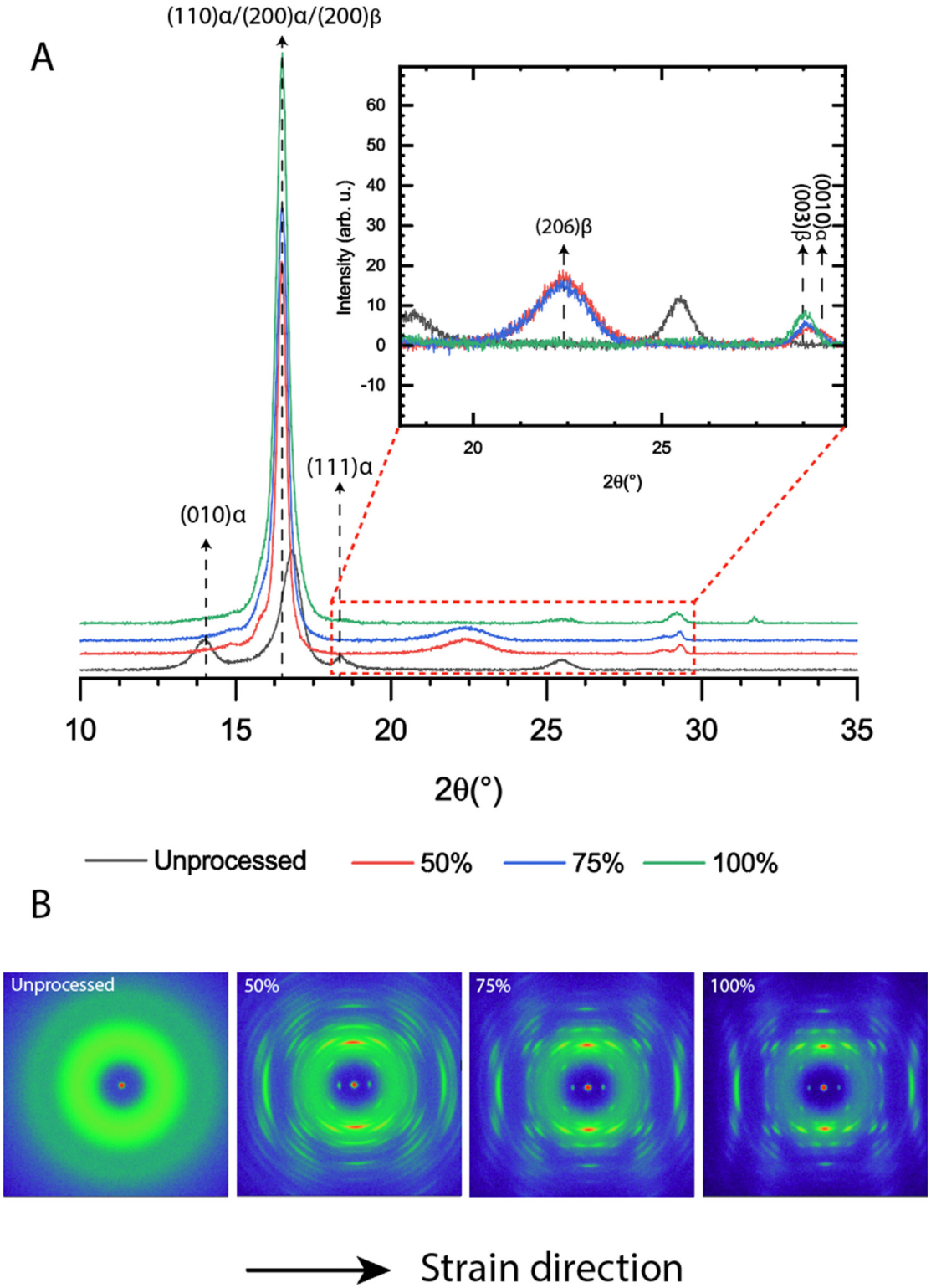

Fig. 5 (A) 1D XRD patterns of PLLA films subjected to various strain levels. Inset shows an enlarged image of the β-phases. (B) two-dimensional WAXS analysis illustrating changes in polymer chain orientation resulting from post-processing with the strain direction.

results. In addition to this, the absorption spectra in PLLA films indicate a correlation between the distinctive peak's intensity and applied strain and suggest a direct influence of crystallinity changes on the spectra. This correlation gains significance in piezoelectric materials, where alterations in crystallinity impact the electric charge generated in response to mechanical deformation. The identified peak corresponds to specific molecular vibrations influencing the material's piezoelectric functionality.

Moreover, a significant increase in the absorption intensity of the distinctive peaks was observed at a rotation angle of 90 degrees for all processed samples for the processed films suggesting that the molecular chains within the processed film are more aligned, resulting in anisotropic behavior that interacts differently with the polarized electric field. This alignment enhances the sensitivity of the absorption spectra to rotational changes, highlighting the influence of molecular orientation and crystallinity on the film's optical properties. Beyond rotational effects, a notable shift to higher frequencies in peak position is observed in the strained films. This slight shift can be attributed to phase transitions within the PLLA crystalline structure, specifically changes in lattice spacing caused by mechanical stretching.[42] Such transitions result in tighter packing within the crystalline regions, further demonstrating the capacity of THz spectroscopy to detect not only orientation-dependent behavior but also structural changes at the molecular level. This finding suggests a pronounced directional sensitivity of PLLA films to the electric field, with enhanced absorption when the electric field is parallel to the strain direction. This heightened absorption when the electric field is parallel to the strain direction suggests that the orientation of polymer chains plays a crucial role in the material's response. To further confirm these phase transitions and the molecular orientation changes indicated by the THz spectroscopy results, XRD and WAXS were employed to provide complementary insights into the crystalline structure and alignment of polymer chains in the processed PLLA films. While traditional techniques such as DSC and XRD are effective for evaluating crystallinity, THz-TDS was introduced in this study as a complementary method, offering enhanced sensitivity to molecular orientation and low-frequency vibrational modes that are closely linked to piezoelectric behavior.

XRD analysis provided detailed insights into the crystallographic changes due to post-processing. The unprocessed PLLA films exhibited crystalline peaks at 14° (010), 16.49° (110)/(200)α/(200)β, and 18.45° (111)α (Fig. 5A). With increasing strain, the 18.45° (111) peak disappeared, while the 16.49° (110)/(200) peaks intensified proportionally to the strain, indicating a transition from the α-form to the β-form, characterized by a 3_1 helical structure.[1,18,43] Additionally, crystallinity peaks at 22.38° (206)β, (003)β and (0010)α were observed in the 50% and 75% strained samples. Furthermore, clear trends were noted at 28.77° (003) and 29.34° (0010). Specifically, the intensity of the (0010) peak diminished with increased strain, suggesting a transformation of the α-phase contribution to the β-phase, consistent with previously reported observations.[43–48] Here, both the α-phase and β-phase exhibit a prominent peak around 16.3–16.6°, which arises from the hexagonal arrangement of the molecular stems, reflecting similar or nearly identical helix-to-helix distances in these two structures.[46] This is especially observed in the case of the 100% strained film. Here, it showed no corresponding peak at (0010)α suggesting the complete transformation to the β-phase contribution. Complementing these findings, 2D WAXS patterns revealed an isotropic distribution of crystalline domains in unprocessed films, which transitioned to well-defined arcs with increasing strain, indicating an anisotropic distribution due to the alignment of crystalline domains in the (200) and (110) directions (Fig. 5B), confirming the results obtained by THz spectroscopy.

The convergence of DSC, FTIR, THz spectroscopy, XRD, and WAXS results provide significant evidence of strain-induced crystalline reorientation and increased crystallinity in PLLA films. The shift to lower melting temperatures and sharper peaks in DSC, alongside the intensified FTIR peaks, corroborates the structural alignment and increased crystallinity observed in XRD and WAXS analyses. The alignment between higher melting temperatures, sharper DSC peaks, intensified FTIR signals, and the disappearance of the (111)α peak, the increased intensity of the (110)/(200)α peaks, and the presence of (003)β peak in XRD, together with the anisotropic alignment shown in WAXS, all point to a comprehensive improvement in the structural integrity and crystallinity of PLLA films under strain.

Quantification of crystallinity using THz-TDS and correlation with XRD and DSC

Building on our analysis of distinctive peaks, an alternative method for quantifying PLLA film crystallinity is explored by fitting classical Lorentzian oscillator models to THz spectra, offering a complementary perspective on molecular dynamics. Hirata *et al.* proposed this method.[29] The main difference is the Dorney correction applied to our THz data for more accuracy and that for the fitting procedure, we used a sum of two Lorentz oscillators instead of three; one to describe the crystallite molecular vibration modes of the PLLA films and the second to describe the vibration modes of the amorphous content. This approach defines the intensity to be the area under the absorption coefficient fit. It considers the crystallinity to be the ratio of the contribution due to the crystal structure by the total intensity (a detailed description of the fitting procedure is presented in the ESI†).

Fig. 5 shows that the crystallinity measurements obtained from the 90-degree rotated THz absorption spectra closely matched those from traditional techniques (XRD and DSC). This alignment demonstrates the accuracy and reliability of using THz-TDS for crystallinity assessment when the straining direction is properly aligned with the electric field. In contrast, when the straining direction was not aligned with the electric field, such as at 50 degrees and 0 degrees, there was a noticeable underrepresentation of crystallinity. This discrepancy may arise because the absorption peaks at these angles are not as pronounced as with the 90-degree rotation, potentially resulting in a poorer fit (see Fig. S2, ESI†). We believe that the stronger vibrational interaction when the samples are aligned parallel to the electric field indicates the direction of alignment of the crystal in the molecule. This stronger interaction likely occurs because the electric field interacts more effectively with the vibrational modes of the crystalline regions when aligned with their orientation, enhancing the interaction and resulting in more pronounced absorption features. These observations highlight the sensitivity of THz-TDS measurements to the sample's orientation relative to the electric field. XRD was used to reinforce the proposition that the crystallinity content in

PLLA films is proportional to the applied strain to validate the THz findings further. This alignment not only enhances the credibility of our study but also establishes a direct link between macroscopic mechanical properties, such as strain, and the material's microscopic structure.

The correlation between XRD and THz findings validates our observations and guides further materials design and optimization, which is essential for enhancing PLLA piezoelectric films for precise mechanical response applications. Quantifying crystallinity using THz-TDS involved measuring the refractive index and absorption coefficients, which are influenced by the degree of molecular order. These changes were correlated to the applied strain, indicating increased molecular alignment. The THz-TDS data correlated well with the crystallinity obtained from XRD and DSC analyses, confirming that increases in birefringence and refractive index were consistent with the crystallinity increases observed in XRD and DSC, see Fig. 6.

The convergence of results from DSC, FTIR, XRD, WAXS, and THz-TDS demonstrates significant strain-induced crystalline reorientation and increased crystallinity in PLLA films. The shift to higher melting temperatures and sharper peaks in DSC (Fig. 2A), alongside the intensified FTIR peaks (Fig. 2B), corroborates the structural alignment and increased crystallinity observed in XRD (Fig. 5A) and WAXS (Fig. 5B) analyses. The alignment between higher melting temperatures, sharper DSC peaks, intensified FTIR signals, the disappearance of the (111) peak, and the increased intensity of the (110)/(200) peaks in XRD, together with the anisotropic alignment shown in WAXS, all point to a comprehensive improvement in the structural integrity and crystallinity of PLLA films under strain. THz-TDS further validated these findings by linking structural changes to electromechanical properties. The observed birefringence and absorption spectra change with strain provided a detailed understanding of the influence of mechanical stretching on molecular orientation and crystallinity, impacting PLLA films' optical and piezoelectric properties. The results from XRD and WAXS confirmed the crystalline alignment observed in the THz-TDS measurements, demonstrating that the intensity of the 16.49° (110)/(200) and (003)β peaks increased with strain, indicating a transition from the α-form to the β-form crystal structure.[1,46] Similarly, 2D WAXS patterns revealed well-defined arcs at higher strains, indicating alignment of crystalline domains in the (200) and (110) directions.

The structural analyses of PLLA films highlight the impact of strain on crystallinity and molecular alignment. To further investigate their electromechanical behavior, piezoresponse force microscopy (PFM) is employed. PFM is a scanning probe technique that measures the local piezoelectric response of materials by applying an AC voltage to a conductive AFM tip in contact mode.[49,50] This voltage induces mechanical vibrations in piezoelectric materials, which are detected as cantilever deflections. The technique provides nanoscale resolution and is widely used to analyze polarization dynamics, ferroelectric domains, and piezoelectric coefficients.[49,50] The piezoelectric

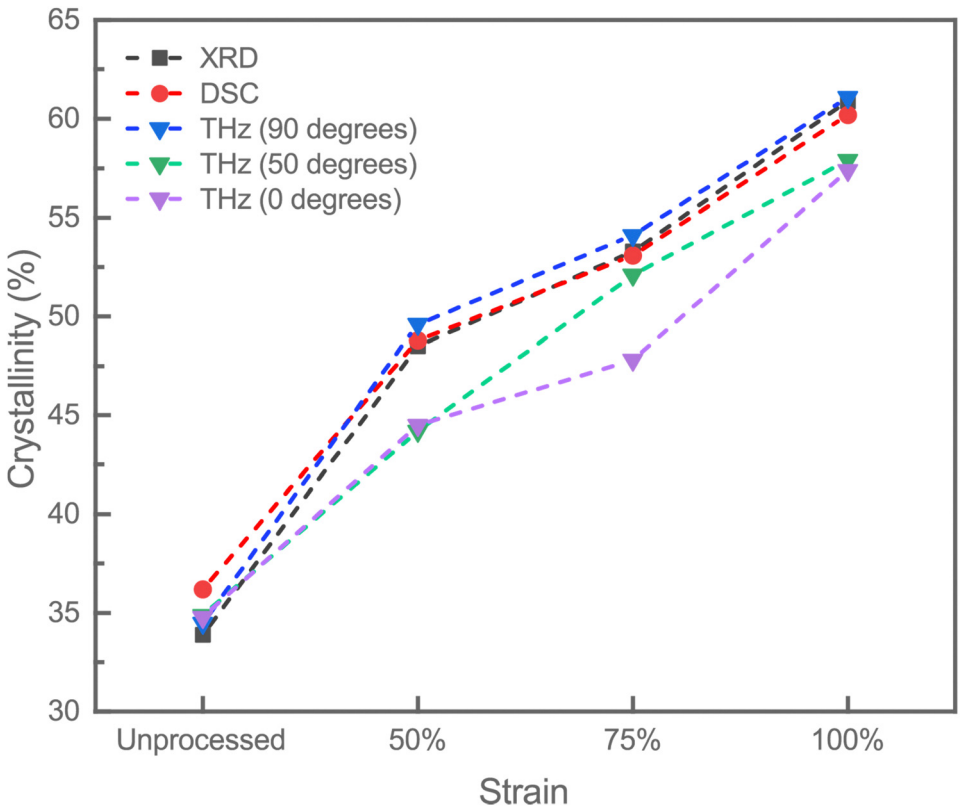

Fig. 6 Crystallinity (%) of PLLA films as a function of strain, comparing results from XRD, DSC, and THz-TDS at different rotational angles (0 degrees, 50 degrees, and 90 degrees).

coefficient is determined by analyzing the relationship between the amplitude of the mechanical response and the applied voltage under calibrated conditions.[49,50] PFM operates in two principal modes: vertical piezoresponse force microscopy (VPFM) and lateral piezoresponse force microscopy (LPFM). VPFM measures the out-of-plane piezoresponse by detecting the vertical deflection of the cantilever, which corresponds to the deformation perpendicular to the sample surface. LPFM, on the other hand, quantifies the in-plane piezoresponse by capturing the torsional oscillations of the cantilever, representing deformation parallel to the surface.[49,51] Here, in our case, LPFM provided valuable insight into the anisotropic behavior of the PLLA films, highlighting strain-induced directional polarization and molecular alignment. These modes enable the differentiation of piezoelectric responses along different material axes, providing a comprehensive understanding of the anisotropic piezoelectric behavior. Although, in this study, LPFM values generally did not show significant changes in comparison to VPFM, their inclusion provided a more complete understanding of piezoelectric properties in the PLLA films, with results depicted in Fig. 7 and piezoelectric characteristics summarized in Table 1. Additional findings, such as detailed characterization, including amplitude and phase imaging, the piezoelectric coefficient, and polarization orientation are presented in the ESI† (Fig. S3), demonstrating the usefulness of PFM in correlating strain-induced structural changes with piezoelectric properties.

For the unprocessed PLLA film, the VPFM response exhibited a modest piezoelectric coefficient of 0.65 ± 0.15 pm V^{-1}, these modest piezoelectric properties can be attributed to the inherent semi-crystalline nature of PLLA. The semi-crystalline regions, consisting of both ordered and amorphous domains, result in limited dipole alignment, which restricts the overall piezoelectric performance. The topographical images confirmed a relatively smooth surface morphology without evident structural alignment, consistent with the absence of external strain, Fig. 7A(1). When analyzed with azimuth angle rotation of 90°, there was no clear indication of directional polarization, reinforcing the lack of alignment in the unstrained film, Fig. 7A(2) confirming previously presented results obtained from WAXS and THz-TDS.

When a 50% strain was applied to the PLLA film, the VPFM piezoelectric coefficient remained consistent with that of the unprocessed film, measuring 0.6 ± 0.2 pm V^{-1}, indicating that the applied strain did not result in a measurable improvement in the piezoelectric output at this stage. However, clear changes in the topography of the material were observed compared to the unprocessed film, suggesting the onset of molecular alignment induced by the applied strain, Fig. 7B.

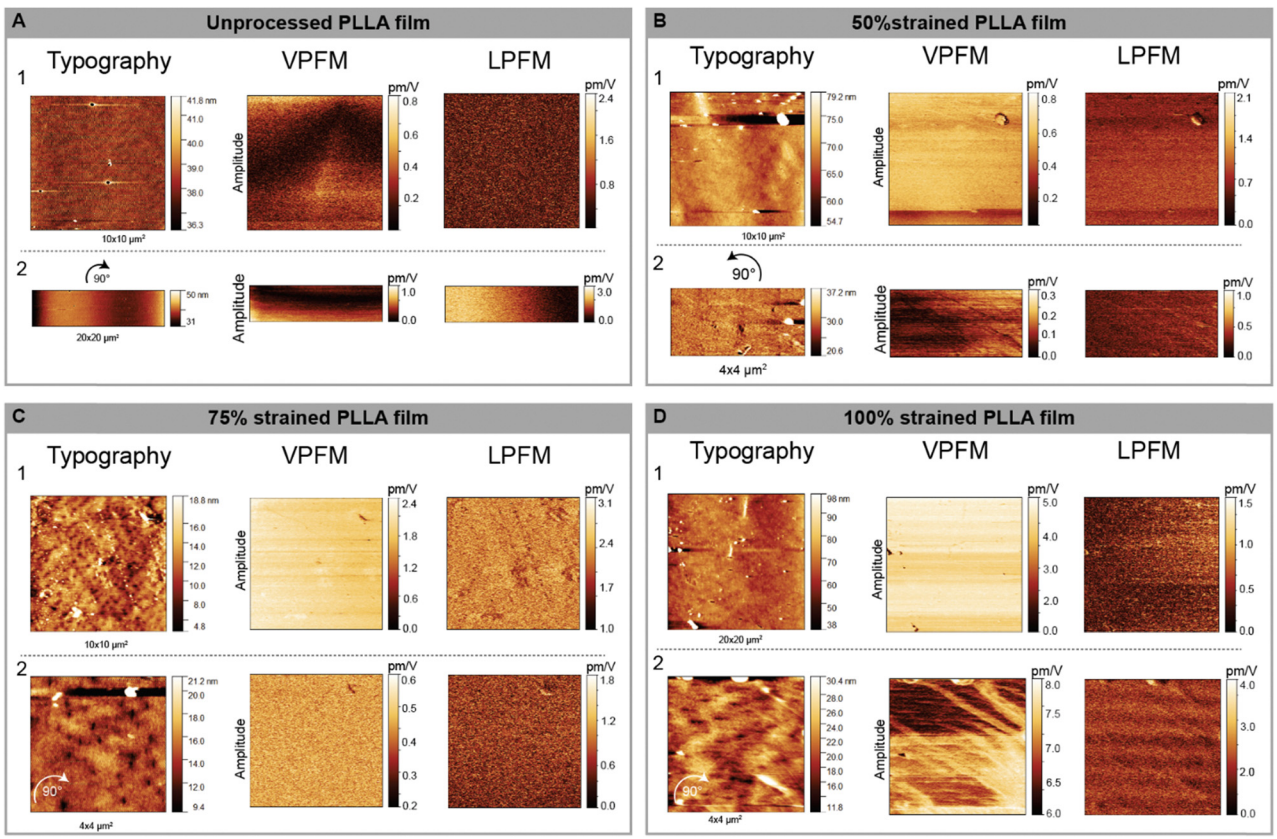

Fig. 7 Scanning probe microscopy analysis of unprocessed (A), 50% (B), 75% (C), and 100% (D) PLLA films. (1) Surface topography (right) and piezo response force microscopy (PFM) images (left) at a scan size of 10 × 10 μm². Corresponding effective piezocoefficient values for vertical (VPFM) and lateral (LPFM) measurements are shown on the left. (2) Surface topography and PFM images (right) after a 90° azimuth angle rotation. Corresponding effective vertical (VPFM) and lateral (LPFM) piezocoefficient values are displayed on the left.

Table 1 Piezoelectric characteristics of unprocessed and strained PLLA films

	Unprocessed	PLLA 50%	PLLA 75%	PLLA 100%
VPFM (pm V^{-1})	0.65 ± 0.15	0.6 ± 0.2	1.4 ± 0.8	6.5 ± 1.5

The 75% strained PLLA film demonstrated a marked increase in VPFM piezo-response, reaching 1.4 ± 0.8 pm V^{-1}, see Fig. 7C(1). Topographical analysis revealed features indicative of molecular alignment, which became more pronounced after azimuth angle rotation of 90°, Fig. 7C(2). Concurrently, LPFM values did not show as dramatic a shift, their inclusion confirmed significant anisotropy. This anisotropy was evident in topography images, particularly at a 4 × 4 μm^2 scan size, as directional alignment became visible. However, the directions for LPFM anisotropy were slightly different from the topographical alignment, which showed primarily horizontal or vertical orientations, Fig. 7C(1). These changes suggest significant molecular alignment in response to the higher strain, enhancing both out-of-plane and in-plane polarization components. In addition to this, this observation indicates the development of directional polarization, as lateral polarization directions became distinctly visible, pointing to alignment along the strain axis. The lateral polarization direction, clearly observed in phase images, is an important indicator of anisotropy, as it reflects the organized molecular dipole structure induced by the applied strain. Finally, the 100% strained PLLA film exhibited a dramatic enhancement in piezoelectric performance. The VPFM piezoelectric coefficient increased significantly to 6.5 ± 1.5 pm V^{-1}. Both the topography images and LPFM analysis supported these findings, as they continued to reinforce the strain-induced anisotropy while maintaining consistency in its directional observations. After azimuth angle rotation of 90°, the data provided strong evidence of directional polarization, with clearly defined lateral polarization patterns, Fig. 7D(2) This further underscores the strain-induced anisotropy in the molecular structure, where the lateral polarization direction is a definitive indicator of the organized alignment.

When drawing these findings back to the results obtained from THz-TDS, XRD, and WAXS, a clearer picture emerges concerning the interplay between crystallinity, molecular alignment, and anisotropy in the strained PLLA films. The THz-TDS results highlighted how crystallinity evolves under strain, with increases in crystalline fraction correlating well with the enhanced piezoelectric coefficients observed at higher strain levels. XRD provided evidence of strain-induced alignment of crystalline domains resulting in the formation of β-form crystal structure resulting in improved piezoelectric properties. These complementary findings highlight the strong relationship between the structural properties of PLLA and its functional performance. The strain-induced anisotropy observed in PFM measurements is a direct consequence of the increased molecular alignment and crystalline fraction, as confirmed by THz-TDS and WAXS. This underscores the potential of PLLA as a tunable material for piezoelectric applications, where its performance can be optimized through controlled strain to achieve the desired degree of crystallinity and molecular alignment.

The results demonstrate the critical role of strain in tuning the piezoelectric properties of PLLA films. The significant increase in piezoelectric coefficients under high strain levels underscores the potential of PLLA as a viable material for piezoelectric applications, particularly in biomedical sensors and actuators. The strain-driven structural organization and the development of anisotropy provide opportunities for designing devices with enhanced sensitivity and functionality tailored for specific applications such as physiological monitoring or energy harvesting. Future studies should focus on refining the strain application process to achieve uniform molecular alignment and on evaluating the stability of piezoelectric properties under dynamic conditions. Additionally, integrating these findings with device-level testing will offer valuable insights into the practical application of PLLA-based piezoelectric systems.

Conclusions

Our study demonstrates that mechanical stretching and thermal annealing enhance the crystallinity and structural alignment of PLLA films. Using a combination of DSC, FTIR, XRD, and WAXS, we consistently observed increased crystallinity with applied strain. Notably, our application of the novel rotational THz-TDS method provided critical confirmation of these results. By rotating the THz-TDS measurements to align the straining direction with the electric field, we achieved crystallinity values that closely matched those obtained from XRD and DSC. Crystallinity increased from 34.8% in unprocessed PLLA films to 44.5%, 47.8%, and 57.4% at strain levels of 50%, 75%, and 100%, respectively. This innovative approach highlighted the importance of alignment for accurate crystallinity measurements and provided additional insights into the material's structural properties. The 90-degree rotated THz absorption spectra validated our findings and emphasized the detailed correlation between molecular orientation and crystallinity. This method offered a complementary evolution of molecular dynamics, enhancing our understanding of how mechanical stretching influences the piezoelectric properties of PLLA films. PFM analysis further corroborated the findings by directly demonstrating the strain-dependent evolution of piezoelectric response in PLLA films. The vertical piezoelectric coefficient increased significantly from 0.65 ± 0.15 pm V^{-1} in unprocessed films to 6.5 ± 1.5 pm V^{-1} at 100% strain, reflecting enhanced molecular alignment and crystallinity under mechanical stretching. Despite the lack of significant changes in LPFM values, its ability to indicate anisotropy complemented the VPFM measurements, providing a more comprehensive understanding of piezoelectric behavior. Azimuth angle rotations confirmed the presence of directional polarization and revealed strain-induced anisotropy, further emphasizing the relationship between molecular structure and piezoelectric performance. These findings highlighted the role of semi-crystalline alignment in tuning piezoelectric properties, thus reinforcing the suitability of PLLA for device applications. The increased crystallinity achieved through post-processing techniques directly correlates with improved piezoelectric response, making PLLA films

highly suitable for advanced biomedical applications. The ability to precisely tune the piezoelectric properties through controlled crystallinity opens new possibilities for developing high-performance, biodegradable piezoelectric devices for various applications.

Data availability

The data supporting this article have been included as part of the ESI.†

Conflicts of interest

The authors declare that they have no known conflicts of interest or competing financial interests that could have influenced the work reported in this paper.

Acknowledgements

The project is funded by the Independent Research Fund Denmark under Grant 1032-00182B. AK acknowledges the project FeLow-D funded under the Horizon Europe programme HORIZON-WIDERA-2023-TALENTS-01, GA no. 101186499. This work was developed within the scope of the project CICECO-Aveiro Institute of Materials, UIDB/50011/2020 (DOI: https://doi.org/10.54499/UIDB/50011/2020), UIDP/50011/2020 (DOI: https://doi.org/10.54499/UIDP/50011/2020) & LA/P/0006/2020 (DOI: https://doi.org/10.54499/LA/P/0006/2020), financed by national funds through the FCT/MCTES (PIDDAC).

References

1 E. J. Curry, *et al.*, Biodegradable Piezoelectric Force Sensor, *Proc. Natl. Acad. Sci. U. S. A.*, 2018, **115**(5), 909–914.
2 Y. Wu, *et al.*, Piezoelectric materials for flexible and wearable electronics: A review, *Mater. Des.*, 2021, **211**, 110164.
3 F. Yang, *et al.*, Electrospinning of nano/micro scale poly(L-lactic acid) aligned fibers and their potential in neural tissue engineering, *Biomaterials*, 2005, **26**(15), 2603–2610.
4 E. Capuana, *et al.*, Poly-L-Lactic Acid (PLLA)-Based Biomaterials for Regenerative Medicine: A Review on Processing and Applications, *Polymers*, 2022, **14**(6), DOI: 10.3390/polym14061153.
5 H. Tsuji, Poly(lactide) stereocomplexes: Formation, structure, properties, degradation, and applications, *Macromol. Biosci.*, 2005, **5**(7), 569–597.
6 A. Khan, *et al.*, The potential of organic piezoelectric materials for next-generation implantable biomedical devices, *NanoTrends*, 2024, 100032.
7 L. Persano, S. K. Ghosh and D. Pisignano, Enhancement and Function of the Piezoelectric Effect in Polymer Nanofibers, *Acc. Mater. Res.*, 2022, **3**(9), 900–912.
8 X. Nan, *et al.*, Review of Flexible Wearable Sensor Devices for Biomedical Application, *Micromachines*, 2022, **13**(9), 1395.
9 F. Yang, *et al.*, Electrospinning of nano/micro scale poly(L-lactic acid) aligned fibers and their potential in neural tissue engineering, *Biomaterials*, 2005, **26**(15), 2603.
10 J.-F. Ru, *et al.*, Dominant β-Form of Poly(l-lactic acid) Obtained Directly from Melt under Shear and Pressure Fields, *Macromolecules*, 2016, **49**(10), 3826–3837.
11 M. Smith, *et al.*, Enhanced Molecular Alignment in Poly-l-Lactic Acid Nanotubes Induced via Melt-Press Template-Wetting, *Macromol. Mater. Eng.*, 2019, **304**(3), 1800607.
12 Y. Merhi and S. Agarwala, Fabrication of flexible, and bioresorbable poly-l-lactide acid piezoelectric material with tunable properties, *Mater. Today: Proc.*, 2022, **70**, 531–534.
13 L. Wu, *et al.*, Piezoelectric materials for neuroregeneration: a review, *Biomater. Sci.*, 2023, **11**(22), 7296–7310.
14 S. Guerin, S. A. M. Tofail and D. Thompson, Organic piezoelectric materials: milestones and potential, *NPG Asia Mater.*, 2019, **11**(1), 10.
15 S. Sasaki and T. Asakura, Helix Distortion and Crystal Structure of the α-Form of Poly(L-lactide), *Macromolecules*, 2003, **36**(22), 8385–8390.
16 H. J. Oh, *et al.*, Fabrication of piezoelectric poly(l-lactic acid)/BaTiO3 fibre by the melt-spinning process, *Sci. Rep.*, 2020, **10**(1), 16339.
17 K. Wasanasuk and K. Tashiro, Crystal structure and disorder in Poly(l-lactic acid) δ form (α′ form) and the phase transition mechanism to the ordered α form, *Polymer*, 2011, **52**(26), 6097–6109.
18 A. Farahani, *et al.*, Polylactic Acid Piezo-Biopolymers: Chemistry, Structural Evolution, Fabrication Methods, and Tissue Engineering Applications, *J. Funct. Biomater.*, 2021, **12**(4), 71.
19 J. Zhang, *et al.*, Disorder-to-Order Phase Transition and Multiple Melting Behavior of Poly(l-lactide) Investigated by Simultaneous Measurements of WAXD and DSC, *Macromolecules*, 2008, **41**(4), 1352–1357.
20 P. Bawuah and J. A. Zeitler, Advances in terahertz time-domain spectroscopy of pharmaceutical solids: A review, *TrAC, Trends Anal. Chem.*, 2021, **139**, 116272.
21 J. A. Zeitler and L. F. Gladden, In-vitro tomography and non-destructive imaging at depth of pharmaceutical solid dosage forms, *Eur. J. Pharm. Biopharm.*, 2009, **71**(1), 2–22.
22 L. Sun, L. Zhao and R. Y. Peng, Research progress in the effects of terahertz waves on biomacromolecules, *Mil. Med. Res.*, 2021, **8**(1), 28.
23 R. Yang, *et al.*, Novel Terahertz Spectroscopy Technology for Crystallinity and Crystal Structure Analysis of Cellulose, *Polymers*, 2021, **13**(1), 6.
24 S. Wietzke, *et al.*, Terahertz spectroscopy on polymers: A review of morphological studies, *J. Mol. Struct.*, 2011, **1006**(1), 41–51.
25 P. D. Cunningham, *et al.*, Broadband terahertz characterization of the refractive index and absorption of some important polymeric and organic electro-optic materials, *J. Appl. Phys.*, 2011, **109**(4), 043505.
26 F. Zhang, *et al.*, Elucidation of Chiral Symmetry Breaking in a Racemic Polymer System with Terahertz Vibrational Spectroscopy and Crystal Orbital Density Functional Theory, *J. Phys. Chem. Lett.*, 2016, **7**(22), 4671–4676.
27 S. Sommer, M. Koch and A. Adams, Terahertz Time-Domain Spectroscopy of Plasticized Poly(vinyl chloride), *Anal. Chem.*, 2018, **90**(4), 2409–2413.

28 H. Iwasaki, *et al.*, Controlled Terahertz Birefringence in Stretched Poly(lactic acid) Films Investigated by Terahertz Time-Domain Spectroscopy and Wide-Angle X-ray Scattering, *J. Phys. Chem. B*, 2017, **121**(28), 6951–6957.
29 J. Hirata, *et al.*, Evaluation of Crystallinity and Hydrogen Bond Formation in Stereocomplex Poly(lactic acid) Films by Terahertz Time-Domain Spectroscopy, *Macromolecules*, 2020, **53**(16), 7171–7177.
30 Z. Zhu, *et al.*, Study of Crystallinity and Conformation of Poly(lactic acid) by Terahertz Spectroscopy, *Anal. Chem.*, 2022, **94**(31), 11104–11111.
31 Z. Zhu, *et al.*, Study on the crystallization behavior and conformation adjustment scale of poly(lactic acid) in the terahertz frequency range, *Phys. Chem. Chem. Phys.*, 2023, **25**(12), 8472–8481.
32 Q. Sun, *et al.*, Recent advances in terahertz technology for biomedical applications, *Quant. Imaging Med. Surg.*, 2017, **7**(3), 345–355.
33 M. Ulmschneider, Terahertz Imaging of Drug Products, in *Infrared and Raman Spectroscopic Imaging*, 2014, pp. 445–476.
34 N. Fuse, *et al.*, Observation and Analysis of Molecular Vibration Modes in Polylactide at Terahertz Frequencies, *Jpn. J. Appl. Phys.*, 2010, **49**(10R), 102402.
35 T. D. Dorney, R. G. Baraniuk and D. M. Mittleman, Material parameter estimation with terahertz time-domain spectroscopy, *J. Opt. Soc. Am. A*, 2001, **18**(7), 1562–1571.
36 J. R. Sarasua, *et al.*, Crystallinity assessment and in vitro cytotoxicity of polylactide scaffolds for biomedical applications, *J. Mater. Sci.: Mater. Med.*, 2011, **22**(11), 2513–2523.
37 X. Li, *et al.*, Effect of stereocomplex crystal and flexible segments on the crystallization and tensile behavior of poly(L-lactide), *RSC Adv.*, 2018, **8**(50), 28453–28460.
38 W. Hoogsteen, *et al.*, Crystal structure, conformation and morphology of solution-spun poly(L-lactide) fibers, *Macromolecules*, 1990, **23**(2), 634–642.
39 X. Du, *et al.*, Study of field-induced chain conformation transformation in poly(L-lactic acid) based piezoelectric film by infrared spectroscopy, *J. Appl. Phys.*, 2016, **120**(16), 164101.
40 E. Meaurio, *et al.*, Conformational Behavior of Poly(l-lactide) Studied by Infrared Spectroscopy, *J. Phys. Chem. B*, 2006, **110**(11), 5790–5800.
41 T. Hasegawa, *Quantitative Infrared Spectroscopy for Understanding of a Condensed Matter*, Springer, Tokyo, 2017.
42 S. Ariyoshi, *et al.*, Temperature dependent poly(l-lactide) crystallization investigated by Fourier transform terahertz spectroscopy, *Mater. Adv.*, 2021, **2**(14), 4630–4633.
43 K. Takahashi, *et al.*, Crystal transformation from the α- to the β-form upon tensile drawing of poly(l-lactic acid), *Polymer*, 2004, **45**(14), 4969–4976.
44 H. Zhou, T. B. Green and Y. L. Joo, The thermal effects on electrospinning of polylactic acid melts, *Polymer*, 2006, **47**(21), 7497–7505.
45 H. M. de Oca and I. M. Ward, Structure and mechanical properties of poly(L-lactic acid) crystals and fibers, *J. Polym. Sci., Part B: Polym. Phys.*, 2007, **45**(8), 892–902.
46 B. Lotz, *et al.*, Crystal polymorphism of polylactides and poly(Pro-*alt*-CO): The metastable beta and gamma phases. Formation of homochiral PLLA phases in the PLLA/PDLA blends, *Polymer*, 2017, **115**, 204–210.
47 L. Su, *et al.*, Influence of different β-nucleation agents on poly(l-lactic acid): structure, morphology, and dynamic mechanical behavior, *RSC Adv.*, 2017, **7**(87), 55364–55370.
48 D. Sawai, *et al.*, Preparation of Oriented β-Form Poly(l-lactic acid) by Solid-State Coextrusion: Effect of Extrusion Variables, *Macromolecules*, 2003, **36**(10), 3601–3605.
49 K. Romanyuk, *et al.*, Single- and Multi-Frequency Detection of Surface Displacements *via* Scanning Probe Microscopy, *Microsc. Microanal.*, 2015, **21**(1), 154–163.
50 K. N. Romanyuk, *et al.*, Local electronic transport across probe/ionic conductor interface in scanning probe microscopy, *Ultramicroscopy*, 2021, **220**, 113147.
51 K. Romanyuk, *et al.*, Piezoactive dense diphenylalanine thin films via solid-phase crystallization, *Appl. Mater. Today*, 2022, **26**, 101261.